Macromolecular Rapid Communication
www.mrc-journal.de

Enzyme Responsive Inverse Opal Hydrogels

*Yi Pei, Thomas G. Molley, and Kristopher A. Kilian**

Structured color in nature is controlled by nano- and micro-structured interfaces giving rise to a photonic bandgap. This study presents a biomimetic optical material based on polymeric inverse opals that respond to enzyme activity. Polymer colloids provide a template in which acryloyl-functionalized poly(ethylene glycol) is integrated; dissolution of the colloids leads to a hydrogel inverse opal that can be lithographically patterned using transfer printing. Incorporating enzyme substrates within the voids provides a material that responds to the presence of proteases through a shift in the optical properties.

Our world is dominated by colors that originate from three main sources: pigment, bioluminescence, and structure coloration.[1] Among these three different sources, structural coloration is caused by the interference of nano- or micro-scale surface structures and visible light. Morpho butterfly, for instance, has scales with a complicated tree-like microstructure that is essential for its blue color.[2] Other examples include the vibrant colors of peacock feathers, metallic reflection of beetles, and the iridescent spines of certain types of sea mice.[3–5] Interestingly, the structural colors in some species are dynamic and can be actively altered depending on changes in environment. Chameleons, for instance, have guanine crystals within a superficial thick layer of dermal iridophores and can regulate their skin colors by adjusting the distance between the guanine crystals.[6]

Inspired by these examples in nature, researchers have tried to replicate dynamic structured color in the laboratory for diverse applications from antireflective coatings to sensors. One promising aspect of these bioinspired materials is the changes in optical properties on account of changes in the materials' structures. This attribute makes bioinspired architectures promising for sensing because a change associated with a specific molecular species, such as small molecules, enzymes, antigen/antibody, or nucleic acids will lead to defined shift in optical properties which can be reported through a remote optical transduction modality.[7–12] The field of optical sensor materials is of broad interest due to potential impact across many different areas, such as environment monitoring, food quality, and advanced health care.[13–15] Concurrent with the rapid advances in nanomaterial fabrication technology, structural colored biosensors which utilize the diffraction and/or reflection of light to transduce biorecognition into an optical signal have the advantages of label-free reporting and tunable response range compared to other biosensors.[15]

To date, researchers have successfully fabricated various biomimetic structural colored materials by both top-down and bottom-up methods.[16] Structured materials for biosensing have included those based on porous silicon (PSi), nanostructured metal oxides, and polymer architectures.[17–22] Among them, polymeric inverse opal structures have drawn considerable attention as prospective sensor materials with demonstrations in monitoring humidity, pH, temperature, glucose, and biological macromolecules.[23–32] More recently, the ability to fabricate large area planar opal and inverse opal materials has made them attractive substrates for cell culture, where changes in optical properties correspond to specific cellular activity.[33–40]

In this communication, we present a synthetic hydrogel-based inverse opal construct that can be micropatterned through lithography and transfer printing, with the ability to monitor the activity of protease enzymes. In contrast to previous work where stretching or swelling of inverse opals leads to optical actuation, here we fill the voids of the inverse opal structure with enzyme-active materials to remotely monitor activity in real time. In this way, the optical response can be tuned simply by tailoring the infiltrating materials to correspond to a desired activity.

To fabricate the opal structure, we assembled closely packed monodisperse poly(methyl methacrylate) (PMMA) spheres as described previously and illustrated in **Figure 1**a.[41] Solutions of PMMA colloids with diameters of 250 nm were pipetted onto the surface of glass cover slips and allowed to self-assemble on a hotplate set to 90 °C. The evaporation of the solvent serves as the driving force for self-assembly and the samples are removed from the hotplate after they are completely dried. Scanning electron microscopy (SEM) confirms the closely packed organization of PMMA spheres and microscopic image of the opal demonstrates a vivid green structural color (Figure 1c). Reflectivity measurements indicate that the sample has a stop band around 555 nm as shown in Figure 1b. The position of the stop band can be calculated by combining Bragg's law with Snell's law:

Dr. Y. Pei, T. G. Molley
School of Materials Science and Engineering
University of New South Wales
Sydney 2052, Australia
K. A. Kilian
School of Materials Science and Engineering
School of Chemistry
Australian Centre for Nanomedicine
University of New South Wales
Sydney 2052, Australia
E-mail: k.kilian@unsw.edu.au
The ORCID identification number(s) for the author(s) of this article can be found under https://doi.org/10.1002/marc.201900555.

DOI: 10.1002/marc.201900555

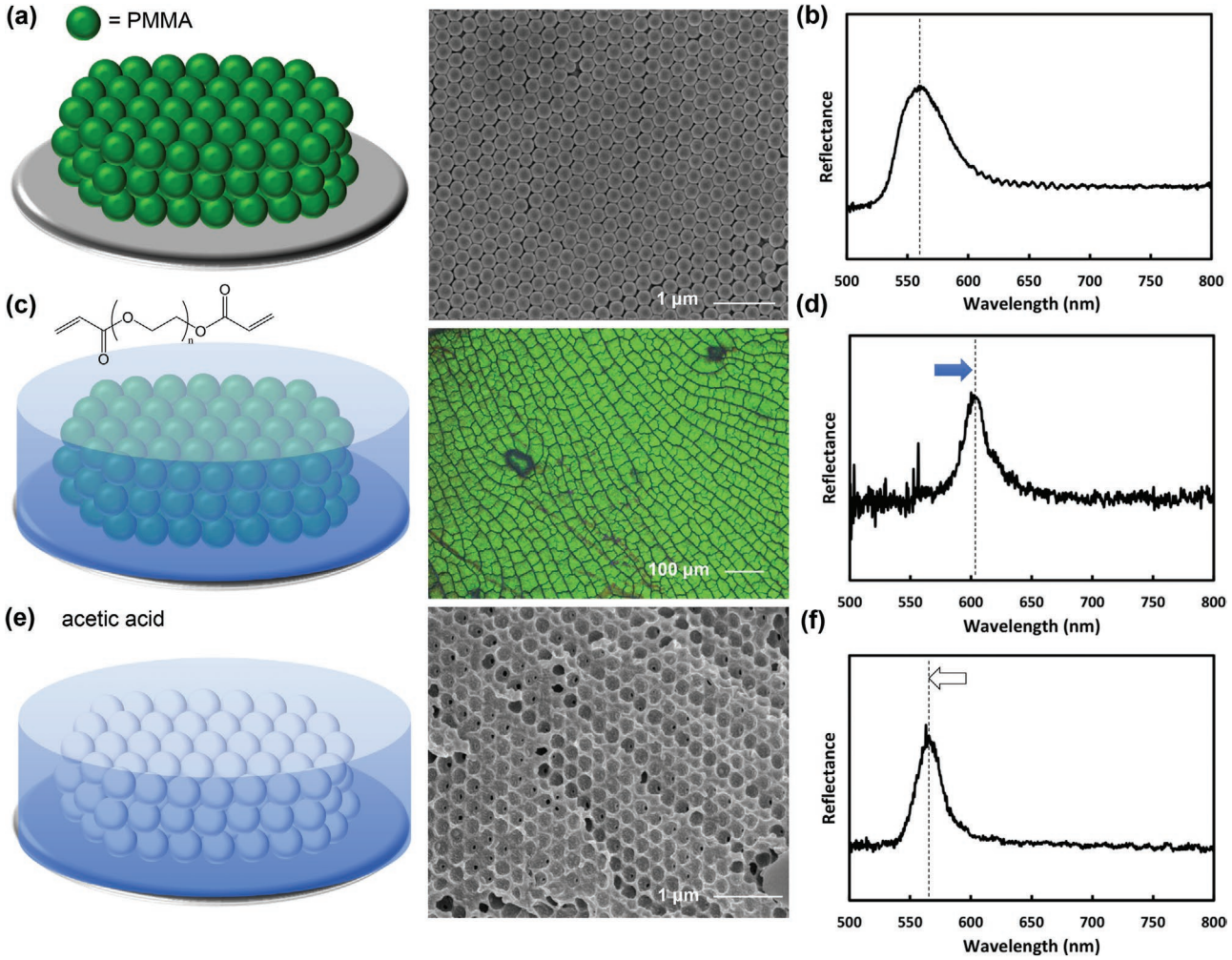

Figure 1. Fabrication of opal and inverse opal hydrogel structures. a) Schematic of opal structure fabricated with 250 nm diameter PMMA colloids and associated scanning electron micrograph (SEM). b) Reflectivity profile of opal structure depicted. c) Schematic of opal structure filled with PEGDA hydrogel and photograph of opal structure. d) Reflectivity profile of opal structure filled with PEGDA hydrogel. e) Schematic of PEGDA inverse opal and associated cross-section SEM. f) Reflectivity profile of PEGDA inverse opal.

$$\lambda = 2d\cos\theta = \left(\frac{8}{3}\right)^{\frac{1}{2}} D\left(n_1{}^2V_1 + n_2{}^2V_2 - \sin^2\theta\right)^{\frac{1}{2}} \quad (1)$$

where D is the distance between diffracting planes; n_1, n_2 are the refractive index of particles and matrix, respectively; V_1, V_2 are the corresponding volume fractions of particles and matrix and have the values of 0.74 and 0.26, respectively, for an ideally packed opal structure; θ is the angle of incident light; θ is kept to zero in our experiment settings. With $n_1 = 1.48$ for PMMA and $n_2 = 1$ for air, the stop band position is expected at $\lambda = 559$ nm, which is consistent with the reflectivity profile.

Accordingly, the increase of average refractive index of the structure will lead to a red shift of the stop band. We next added a solution of polyethylene glycol diacrylate (PEGDA, $M_W = 700$) to fill the voids of the opal structure via capillary forces followed by polymerization under UV light (Figure 1c). In agreement with theory, the stop band of the opal shifts to 600 nm after PEGDA infiltration, as shown in Figure 1d, suggesting replacement of air in the opal with high refractive index organic material (PEGDA700 $\eta = 1.47$; PEGDMA10000 $\eta = 1.46$). The PMMA template was then removed by dissolution with acetic acid and the resulting inverse opal thin film was washed and preserved in DI water for further usage. The schematic of inverse opal and its reflectivity profile are shown in Figure 1e,f. Similar to the discussion before, the replacement of PMMA spheres with DI water leads to the decrease of average refractive index in the optical system and the stop band undergoes a blue shift to 563 nm (Figure 1f). The SEM image also confirms the successful removal of PMMA spheres which is evident by the empty cavities in the hydrogel matrix. SEM indicates some shrinkage of the cavities after removal of the 250 nm PMMA particles to approximately 218 +/− 2.2 nm. However, this may be related to the critical point drying and high-vacuum conditions of the SEM. There is some indication of minor residual PMMA within the structure; however, the reproducible blue-shift after acid treatment indicates successful fabrication of the inverse architecture. Figure S1, Supporting Information,

presents the data of opal and inverse opal made from 300 nm PMMA spheres. The peak positions are at higher wavelengths due to the increase of the distance between refracting planes. It is also not surprising that by changing the concentration of the PEGDA solution, the stop band position of inverse opal will change accordingly, due to the alteration of the refractive index of PEGDA gel. Figure S2, Supporting Information, shows the peak positions of PEGDA inverse opal at various concentrations. The higher the concentration, the higher the wavelength at which the stop band is positioned. Therefore, the signal position can be finely tuned on demand through selection of PMMA sphere size and hydrogel concentration.

For device fabrication and biosensor applications, control over positioning and generation of an array of sensor elements is often desired. Lithographic patterning has proved an enormously useful technique to control the spatial patterning of nano- and micro-scale objects and for increasing the throughput of sensing assays.[42–44] To explore the possibility of fabricating inverse opal hydrogel arrays, we developed a method to pattern our inverse opal films through a transfer printing approach. Specifically, SU8 photoresist was spin coated on a silicon wafer and then patterned through optical lithography to create a master with desired features patterned in relief. PMMA spheres were subsequently deposited on top of the master and allowed to self-assemble into an opal structure at the base of each feature. Excess PMMA spheres on the SU8 surface were carefully removed with an adhesive film before the hydrogel solution was added. After UV cross linking, the hydrogel films were lifted off of the surface and immersed in acetic acid solution with shaking for 48 h. As shown in **Figure 2**, PEGDA filled PMMA (Figure 2a,b) and PEGDA inverse opal (Figure 2c,d) can be made into different shapes with controlled spacing. As expected, the surface morphology of the patterns, either PEGDA filled opal (Figure 2e) or PEGDA inverse opal (Figure 2g), are different to the nonpatterned area (Figure 2f,h). Microscopic images and reflectivity data verify the resonances before (Figure 2i,j) and after (Figure 2k,l) removal of the PMMA template.

Having fabricated planar and patterned inverse opal hydrogel structures, we next explored the suitability of these optical films for sensing. Since changing the refractive index of the surrounding and infiltrating material leads to well-defined shifts in the optical properties, we evaluated introduction of a bio-responsive material into the pores of the inverse opal films. We note that during the fabrication of PEGDA inverse opal films, excess PEGDA solution may lead to highly cross-linked bulk PEGDA

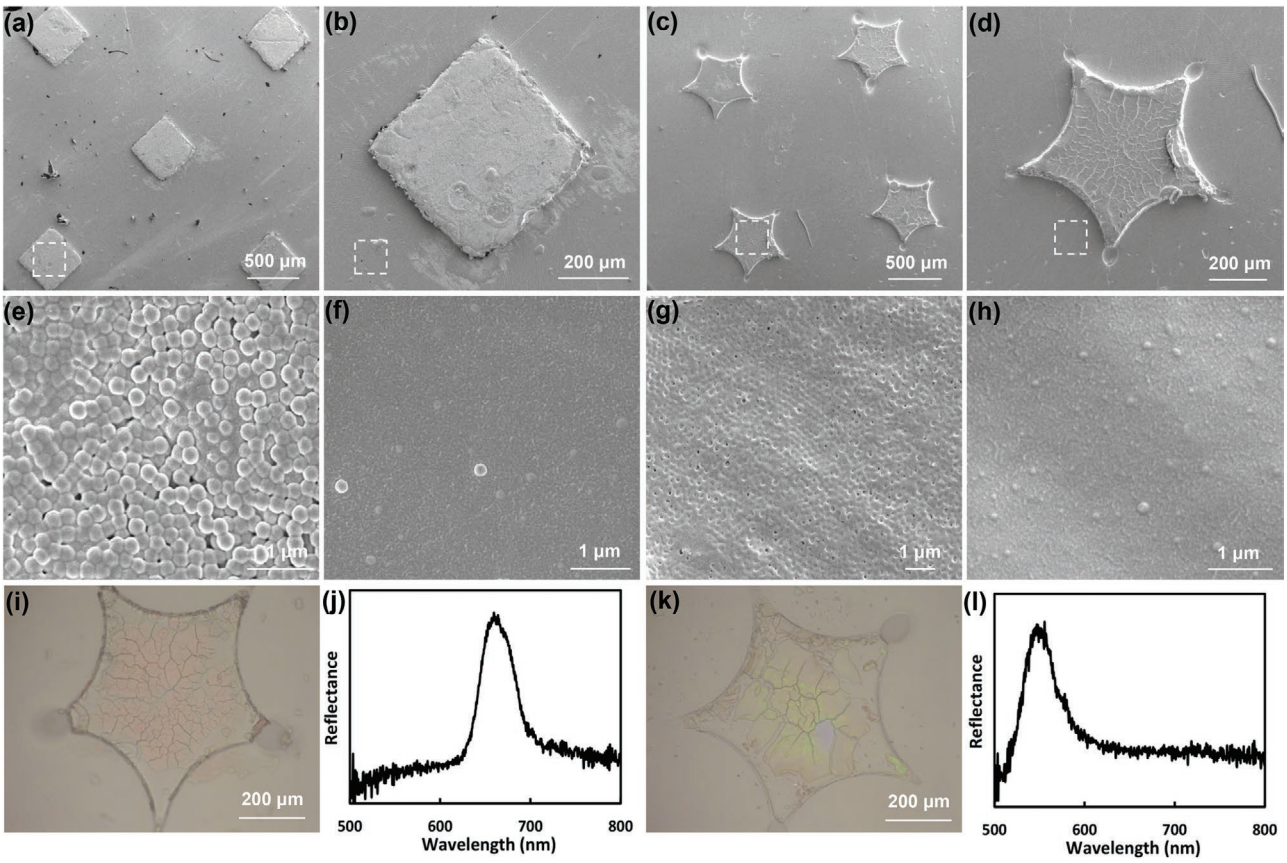

Figure 2. Lithographic printing of inverse opal arrays. a,b) SEM images of patterned PMMA spheres filled with PEGDA. c,d) SEM images of patterned PEGDA inverse opal. e) SEM image of the patterned surface of the infiltrated sample. f) SEM image of the unpatterned surface of the infiltrated sample. g) SEM image of the patterned surface of inverse opal. h) SEM image of the unpatterned surface of inverse opal sample. i) Microscopic image of infiltrated sample. j) Reflectivity profile of infiltrated sample. k) Microscopic image of inverse opal. l) Reflectivity profile of inverse opal. Panels (a), (b), (e), (f), (i), and (j) are data collected from samples made of 300 nm PMMA spheres, while (c), (d), (g), (h), (k), and (l) are data collected from samples made of 250 nm PMMA spheres.

gels forming on both sides of the film as shown in Figure S3, Supporting Information. In this case, access to the pores of the inverse opal film is impeded by the PEGDA hydrogel at the interface. Therefore, it is important that introduced molecular species can infiltrate through the polymer network. Indeed, our initial attempts at infiltrating gelatin biopolymers into opals formed with PEGDA did not result in appreciable penetration as determined by monitoring the reflectivity spectra. In order to formulate a polymer mixture with appropriate diffusional properties, a high-molecular-weight polyethylene glycol dimethacrylate (PEGDM, M_W = 10 kDa) was mixed with PEGDA (M_W = 700) at 1:1 ratio to reduce the number of crosslinks per unit volume for ease of macromolecular diffusion. **Figure 3**a shows the schematic and reflectivity data of the resulting polyethylene glycol (PEG) inverse opal. Gelatin methacrylate (GelMA) is a commonly used biopolymeric material that has the advantages of defined and controllable crosslinking chemistry, well-established enzyme degradability, as well as the property of encouraging cell attachment.[45] We added 15% GelMA solution to infiltrate the PEGDA+PEGDM inverse opal films. 15% was selected, as this high concentration leads to a large red-shift on infiltration, which will also allow higher sensitivity through degradation-mediated blue shifts in the spectrum. As shown in Figure 3b, after the infiltration of GelMA, the stop band red shifts around 40 nm due to the increase of average refractive index. We also explored the generality of the approach by infiltrating the PEG inverse opal with other hydrogel-based materials (Figure S4, Supporting Information). In support of the optical sensing modality, the infiltration of pure PEGDA leads to a disappearance of the optical resonance, since the infiltrating material refractive index is the same as the inverse opal material.

Matrix metalloprotease enzymes, including the gelatinases, are responsible for remodeling of the extracellular matrix during normal and pathological processes.[46] To explore the ability of our inverse opal materials to detect protease activity, we incubated samples in different concentrations of collagenase

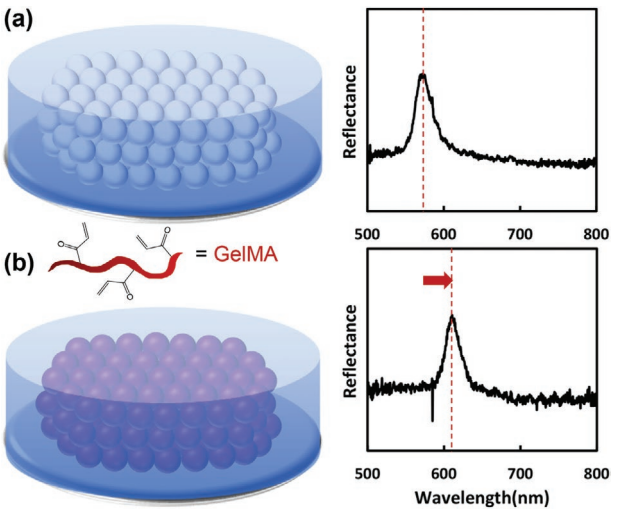

Figure 3. Infiltration of GelMA as an enzyme substrate into the inverse opal. a) Schematic of inverse opal and associated reflectivity profile. b) Schematic of GelMA infiltrated inverse opal and associated reflectivity profile.

solution. Samples were immersed in phosphate-buffered saline (PBS) and 0.1, 0.2, 0.5, 1, and 2 μM collagenase solutions and cultured at 37 °C for 0.5, 1, 2, 3, and 4 h. **Figure 4**a demonstrates a fast optical response to 0.5 μM collagenase solution, where the blue shift stabilizes after 2 h. The final position of the stop band is comparable to the initial peak position of the inverse opal film prior to GelMA infiltration, indicating complete degradation by collagenase. Exposure to collagenase leads to a pronounced blue shift compared to the control PBS (Figure 4b); each data point represents the average of four measurements. When we compare collagenase solutions across different concentrations (Figure 4c), it is clear that the blue shifts in the stop bands are dependent on concentration/activity. In order to account for sample variations and environmental factors, a shift ratio can be used for analysis. Shift ratio (R) is calculated as: $R = \frac{\Delta\lambda_{\text{Collagenase}} - \Delta\lambda_{\text{PBS}}}{\Delta\lambda_{\text{GelMA}}}$, where $\Delta\lambda_{\text{collagenase}}$ is the blue shift of the stop band after the sample is cultured in collagenase solution for a certain amount of time; $\Delta\lambda_{\text{PBS}}$ is the shift of the control sample; $\Delta\lambda_{\text{GleMA}}$ is the initial red shift when GelMA is infiltrated into inverse opal film. Figure S5a, Supporting Information, plots shift ratio against time under various culture conditions. Note that 0.1 μM collagenase can cause an obvious shift in less than 30 min. Figure S5b, Supporting Information, indicates that the initial velocity increases with the increase of collagenase concentration in the range of 0.1 to 2 μM. A more detailed kinetic analysis will need to be conducted in order to determine the suitability for this inverse opal architecture for real-time monitoring of enzyme activity.

We have demonstrated fabrication of inverse opal structures using PEG and gelatin-based acryloyl functionalized polymers, and their integration with microfabrication technologies. Our approach provides a general methodology where commonly used hydrogels may be fabricated to display optical properties towards "smart" biomaterials. Here, we show how incorporating GelMA into the void space will lead to red shifting in the optical properties, where introduction of protease enzyme leads to substrate digestion, accompanied by a blue shift toward the original position. Future scope includes the integration of a wide array of substrate biopolymers spanning diverse enzyme activities. Furthermore, a spectral peak shift is not the only potential read-out from this material. For instance, the peak will disappear if the infiltrating material has a comparable refractive index, and the peak may reappear with the presence of stimuli. Considering the wide use of PEG and gelatin-based hydrogels, this system could be easily incorporated into virtually any hydrogel biomaterial assembly to provide an integrated optical readout.

Experimental Section

Materials: All chemicals were purchased from Sigma-Aldrich, unless otherwise specified. The PMMA particles are purchased from Phosphorex Inc. in sizes of 250 and 300 nm with mondispersity specifications verified by the vendor. RainX was purchased from Rain-X.

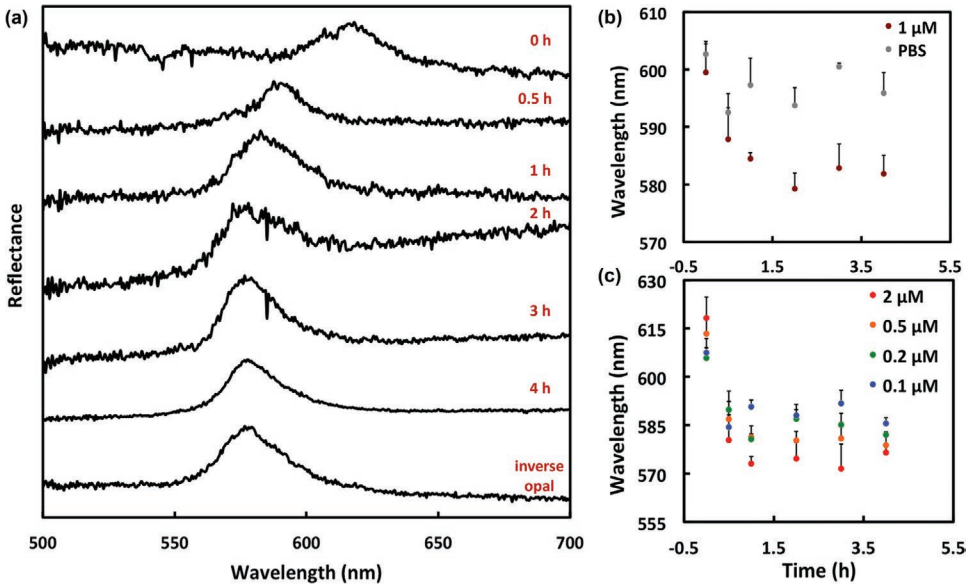

Figure 4. GelMA infiltrated inverse opal structures respond to protease enzymes. a) Shift of the stop band of GelMA-infiltrated PEG inverse opal when cultured in 0.5 μM collagenase solution. b) Comparison of stop band positions when immersed in 1 μM collagenase solution and PBS. c) Comparison of stop band positions when immersed in collagenase of various concentrations.

PEGDM Fabrication: PEGDM was synthesized as reported previously with slight modifications.[47] Briefly, 10 kDa PEG (25g, 2.5 mmol) was dissolved in toluene (125mL) and reduced under vacuum in a rotary evaporator three times. The PEG was subsequently dissolved in toluene (37.5 mL) and dichloromethane (62.5 mL) and reacted with 2.2 equivalents of methacrylic anhydride (846mg, 5.5 mnol) with triethylamine (290 mg, 2.85 mmol) for 48 h under stirring. Potassium carbonate (6.25 g) was used to quench the reaction followed by filtration and precipitation of the PEGDM via the addition of diethyl ether (200 mL). The powder was vacuum filtered, freeze dried, and stored at −20 °C until further use.

GelMA Fabrication: Methacrylated gelatin was synthesized as described previously with slight modifications.[48] Briefly, Type A 300 bloom gelatin was mixed into 1x PBS at 50 °C and stirred until dissolved completely. Next, 0.6 g of methacrylic anhydride was subsequently added dropwise to the solution while stirring at 50 °C and allowed to react for 1.5 h. Following a 4:1 dilution with additional PBS to quench the reaction, the mixture was dialyzed in 14 kDa dialysis tubing for 5–7 days at 40 °C with daily water replacements. The solution was finally lyophilized at −80 °C and stored in the freezer for further use.

Opal Fabrication: Glass cover slips were put onto a hot plate set at 90 °C. 20 μL of 1% PMMA spheres solution was pipetted onto each glass cover slip. The PMMA spheres then self-assembled into opal structures on cover slips by vapor evaporation. The cover slips were removed after the opals were formed.

Inverse Opal Hydrogel Fabrication: 50% PEGDA (M_w = 700 Da) or 30% PEGDA (M_w = 700 Da) + 30% PEGDM (M_w = 10000 Da) solution (v/v) was degassed under argon for 15 min before UV initiator Irgacure (final concentration 0.1% v/v) was added. Glass slides were washed with DI water and ethanol before treated with RainX to create hydrophobic surface. Two pieces of transparent adhesive tape was then attached to the glass slide, leaving a 10 mm gap in between. Cover slips with opal structures on it were then placed right on top of the 10 mm gap with opal structure facing down. 10 μL of PEGDA solution was added to the side of the cover slip and the pre-gelled solution was allowed to infiltrate into the opal structure via capillary force. The glass slide was then transferred into a UV curing chamber and PEGDA gel was formed after 12 min under UV. The cover slip together with PEGDA gel was then lifted up from the glass slide and put into acetic acid to shake for 48 h. The PEGDA gel film was washed thoroughly three times with DI and kept in DI before use.

Infiltration of GelMA: 15 wt% GelMA solution was made and degassed under argon for 15 min before UV initiator Irgacure (final concentration 0.1%) was added. The inverse opal hydrogel was dried briefly through edge contact with a Kimwipe, followed by immersion in GelMA solution at 37 °C for 1 h. The inverse opal hydrogel was then removed from GelMA solution and put under UV for 6 min to facilitate gelation.

SEM Sample Preparation: Inverse opal hydrogels were immersed in 30%, 50%, 70%, 90%, and 100% EtOH, respectively, till equilibrium was reached for each concentration. The samples were then moved into a critical point drying machine (Tousimis Autosamdri-815) per manufacturer's instructions. Samples were mounted and coated with 15 nm of gold before imaging.

Patterning Inverse Opals: Silicon patterned masters of photoresist were created by spin-coating SU-8 followed by UV photolithography through a laser printed mask as described previously.[49] The master was treated by RainX before aliquots of PMMA sphere solution were added on top of the patterns and allowed to form opals. Opals deposited on top of SU-8 were removed with shearing by adhesive tape. A cover slip was then put on top of opals and a drop of PEGDA solution was added adjacent to the cover slip to enable infiltration. The sample was put under UV for 12 min before immersion in acetic acid to remove the PMMA template.

Supporting Information

Supporting Information is available from the Wiley Online Library or from the author.

Acknowledgements

This work was supported by the Australian Research Council award FT180100417.

Conflict of Interest

The authors declare no conflict of interest.

Keywords

biodegradable, biomaterials, biomimetic materials, enzymes, hydrogel

Received: October 21, 2019
Revised: December 19, 2019
Published online: January 31, 2020

[1] J. Sun, B. Bhushan, J. Tong, *RSC Adv.* **2013**, *3*, 14862.
[2] A. Ingram, A. Parker, *Philos. Trans. R. Soc. B: Biol. Sci.* **2008**, *363*, 2465.
[3] J. Zi, X. Yu, Y. Li, X. Hu, C. Xu, X. Wang, X. Liu, R. Fu, *Proc. Natl. Acad. Sci. U. S. A.* **2003**, *100*, 12576.
[4] J. Sun, B. Bhushan, *RSC Adv.* **2012**, *2*, 12606.
[5] R. C. McPhedran, N. A. Nicorovici, D. R. McKenzie, L. C. Botten, A. R. Parker, G. W. Rouse, *Aust. J. Chem.* **2001**, *54*, 241.
[6] J. Teyssier, S. V. Saenko, D. van der Marel, M. C. Milinkovitch, *Nat. Commun.* **2015**, *6*, 6368.
[7] K. Lee, S. A. Asher, *J. Am. Chem. Soc.* **2000**, *122*, 9534.
[8] Q. Zhong, Z. Xie, H. Ding, C. Zhu, Z. Yang, Z. Gu, *Small* **2015**, *11*, 5766.
[9] M. M. F. Choi, *Microchim. Acta* **2004**, *148*, 107.
[10] P. Damborsk´y, D. Damborsk´y, J. J. Jurajšvitel, J. Katrlík, *Essays Biochem.* **2016**, *60*, 91.
[11] M. N. Velasco-Garcia, *Semin. Cell Dev. Biol.* **2009**, *20*, 27.
[12] H.-I. Peng, B. L. Miller, *Analyst* **2011**, *136*, 436.
[13] C. I. L. Justino, A. C. Duarte, T. A. P. Rocha-Santos, *Sensors* **2017**, 17.
[14] M. S. Thakur, K. V Ragavan, *J. Food Sci. Technol.* **2013**, *50*, 625.
[15] S. Patel, R. Nanda, S. Sahoo, E. Mohapatra, *Biochem. Res. Int.* **2016**, *2016*, 3130469.
[16] C. Fenzl, T. Hirsch, O. S. Wolfbeis, *Angew. Chem., Int. Ed.* **2014**, *53*, 3318.
[17] A. Jane, R. Dronov, A. Hodges, N. H. Voelcker, *Trends Biotechnol.* **2009**, *27*, 230.
[18] S. Dhanekar, S. Jain, *Biosens. Bioelectron.* **2013**, *41*, 54.
[19] B. Gupta, Y. Zhu, B. Guan, P. J. Reece, J. J. Gooding, *Analyst* **2013**, *138*, 3593.
[20] Y. Pei, S. H. Shahoei, Y. Li, P. J. Reece, E. R. Nelson, J. J. Gooding, K. A. Kilian, *Adv. Mater. Interfaces* **2018**, *5*, 1801233.
[21] B. D. Malhotra, M. Das, P. R. Solanki, *J. Phys.: Conf. Ser.* **2012**, *358*, 012007.
[22] S. Jung, J. L. Kaar, M. P. Stoykovich, *Mol. Syst. Des. Eng.* **2016**, *1*, 225.
[23] R. A. Barry, P. Wiltzius, *Langmuir* **2006**, *22*, 1369.
[24] B. Yu, H. Cong, Z. Yang, S. Yang, Y. Wang, F. Zhai, Y. Wang, *Materials* **2017**, *10*, 1035.
[25] J. Shin, P. V Braun, W. Lee, *Sens. Actuators, B* **2010**, *150*, 183.
[26] Y.-J. Lee, P. V. Braun, *Adv. Mater.* **2003**, *15*, 563.
[27] J. Shin, S. G. Han, W. Lee, *Sens. Actuators, B* **2012**, *168*, 20.
[28] Y. J. Lee, S. A. Pruzinsky, P. V Braun, *Langmuir* **2004**, *20*, 3096.
[29] L. Jin, Y. Zhao, X. Liu, Y. Wang, B. Ye, Z. Xie, Z. Gu, *Soft Matter* **2012**, *8*, 4911.
[30] J. P. Couturier, M. Sütterlin, A. Laschewsky, C. Hettrich, E. Wischerhoff, *Angew. Chem., Int. Ed.* **2015**, *54*, 6641.
[31] C. I. Aguirre, E. Reguera, A. Stein, *Adv. Funct. Mater.* **2010**, *20*, 2565.
[32] K. R. Phillips, G.T. England, S. Sunny, E. Shirman, T. Shirman, N. Vogel, J. Aizenberg, *Chem. Soc. Rev.* **2016**, *45*, 281.
[33] P. Tseng, S. Zhao, A. Golding, M. B. Applegate, A. N. Mitropoulos, D. L. Kaplan, F. G. Omenetto, *ACS Omega* **2017**, *2*, 470.
[34] F. Fu, L. Shang, Z. Chen, Y. Yu, Y. Zhao, *Sci. Rob.* **2018**, *3*, eaar8580.
[35] Y. Shang, Z. Chen, F. Fu, L. Sun, C. Shao, W. Jin, H. Liu, Y. Zhao, *ACS Nano* **2019**, *13*, 796.
[36] Z. Zhao, J. Wang, J. Lu, Y. Yu, F. Fu, H. Wang, Y. Liu, Y. Zhao, Z. Gu, *Nanoscale* **2016**, *8*, 13574.
[37] A. Stein, B. E. Wilson, S. G. Rudisill, *Chem. Soc. Rev.* **2013**, *42*, 2763.
[38] M. Gallei, *Macromol. Rapid Commun.* **2018**, *39*, 1700648.
[39] T. Winter, X. Su, T. A. Hatton, M. Gallei, *Macromol. Rapid Commun.* **2018**, *39*, 1800428.
[40] C. G. Schafer, T. Winter, S. Heidt, C. Dietz, T. Ding, J. J. Baumbergc, M. Gallei, *J. Mater. Chem. C* **2015**, *3*, 2204.
[41] S. Kim, A. N. Mitropoulos, J. D. Spitzberg, H. Tao, D. L. Kaplan, F. G. Omenetto, *Nat. Photonics* **2012**, *6*, 818.
[42] M. Kitsara, D. Goustouridis, S. Chatzandroulis, M. Chatzichristidi, I. Raptis, T. Ganetsos, R. Igreja, C. Dias, *Sens. Actuators, B* **2007**, *127*, 186.
[43] E. Bat, J. Lee, U. Y. Lau, H. D. Maynard, *Nat. Commun.* **2015**, *6*, 6654.
[44] H. Hong, W. Koom, W. G. Koh, *Sensors* **2017**, *17*, 1293.
[45] J. W. Nichol, S. T. Koshy, H. Bae, C. M. Hwang, S. Yamanlar, A. Khademhosseini, *Biomaterials* **2010**, *31*, 5536.
[46] C. Bonnans, J. Chou, Z. Werb, *Nat. Rev. Mol. Cell Biol.* **2014**, *15*, 786.
[47] S. Lin-Gibson, S. Bencherif, J. A. Cooper, S. J. Wetzel, J. M. Antonucci, B. M. Vogel, F. Horkay, N. R. Washburn, *Biomacromolecules* **2004**, *5*, 1280.
[48] J. W. Nichol, S. T. Koshy, H. Bae, C. M. Hwang, S. Yamanlar, A. Khademhosseini, *Biomaterials* **2010**, *31*, 5536.
[49] J. Lee, A. A. Abdeen, K. L. Wycislo, T. M. Fan, K. A. Kilian, *Nat. Mater.* **2016**, *15*, 856.